Support came from the Deutsche Forschungsgemeinschaft and the Human Frontier Science Program (R.K.), Karolinska Institute, the National Institute of Neurological Disorders and Stroke, The Danish Medical Research Council, and Novo Foundation (O.K), the Swedish Research Council (K.K. and O.K.), European Community Training and Mobility of Researchers grants (K.K. and R.K.), and the Fulbright Foundation (J.L.). K.K. is a Marie Curie Fellow.

Supporting Online Material
www.sciencemag.org/cgi/content/full/299/5614/1889/DC1

Materials and Methods
Figs. S1 to S4
References

22 October 2002; accepted 19 February 2003

Identifying Kinetic Barriers to Mechanical Unfolding of the *T. thermophila* Ribozyme

Bibiana Onoa,[1]*† Sophie Dumont,[2]* Jan Liphardt,[3,4] Steven B. Smith,[1] Ignacio Tinoco Jr.,[3,4] Carlos Bustamante[1,2,3,4]‡

Mechanical unfolding trajectories for single molecules of the *Tetrahymena thermophila* ribozyme display eight intermediates corresponding to discrete kinetic barriers that oppose mechanical unfolding with lifetimes of seconds and rupture forces between 10 and 30 piconewtons. Barriers are magnesium dependent and correspond to known intra- and interdomain interactions. Several barrier structures are "brittle," breakage requiring high forces but small (1 to 3 nanometers) deformations. Barrier crossing is stochastic, leading to variable unfolding paths. The response of complex RNA structures to locally applied mechanical forces may be analogous to the responses of RNA during translation, messenger RNA export from the nucleus, and viral replication.

Numerous cellular processes, such as the translocation of mRNA through the ribosome and the action of RNA helicases and of RNA-dependent RNA polymerases, involve mechanical deformation and unfolding of RNA. Although the structure of RNAs and their folding thermodynamics and kinetics have been the focus of considerable inquiry, it has proven difficult to investigate their molecular responses to mechanical forces. Here, we use optical tweezers (*1*–*3*) to determine the strength and location of kinetic barriers opposing the unfolding of single molecules (*4*, *5*) of the L-21 derivative of the *Tetrahymena thermophila* ribozyme (*6*–*8*), a 390-nucleotide (nt) catalytic RNA (Fig. 1A) whose three-dimensional structure (*9*), independently folding domains (*10*), intra- and interdomain contacts (*11*), and Mg^{2+}-mediated tertiary interactions are well established.

Figure 1B shows a typical force/extension curve obtained by unfolding and refolding a ribozyme molecule in Mg^{2+}. The unfolding curve (black) shows six transitions corresponding to successive unfolding events. Thus, RNA unfolding in the presence of Mg^{2+} and at loading rates of 3 to 5 pN s^{-1} is a "stick-slip" process (*12*): Unfolding temporarily arrests at kinetic barriers (arrows in Fig. 1B) until they yield, leading to a sudden increase in the extension of the RNA and a drop in the force. We refer to these features as "rips" and interpret them as the rapid unfolding of RNA domains. The refolding curve (pink) does not have rips, and thus the unfolding-refolding process in the presence of Mg^{2+} is hysteretic.

When the molecule is unfolded in the absence of Mg^{2+}, the unfolding and refolding curves superpose and the process is reversible. These unfolding and refolding curves are indistinguishable from the refolding curves in Mg^{2+} (Fig. 1B, pink curve) and display a plateau between 10 and 13 pN that is consistent with the progressive unzipping of secondary structure (*13*–*15*). The free energy difference between the folded and unfolded forms of L-21, obtained from the area under the reversible force/extension curves, is $\Delta G_{298K} = 1050 \pm 100$ kJ mol^{-1}, in agreement with a semiempirical free energy calculation (Mfold) when the latter is corrected for

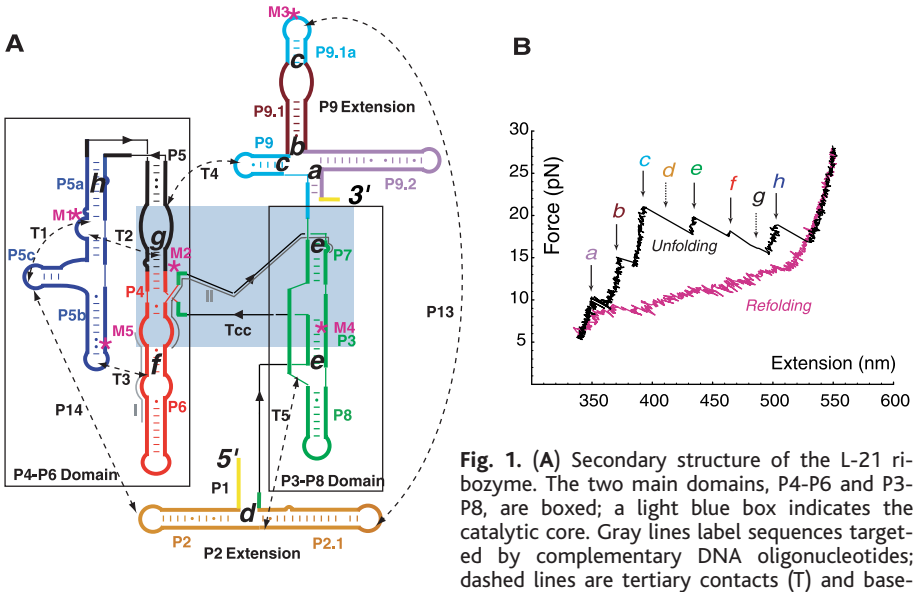

Fig. 1. (**A**) Secondary structure of the L-21 ribozyme. The two main domains, P4-P6 and P3-P8, are boxed; a light blue box indicates the catalytic core. Gray lines label sequences targeted by complementary DNA oligonucleotides; dashed lines are tertiary contacts (T) and base-paired regions (P); "M" labels are site-directed mutations (M1, A to U at site 186; M2, C to G at 260; M3, UGC to ACG at 348 to 350; M4, U to A at 273; M5, cyclic permutation at 148); cc is the catalytic core. The letters *a*, *b*, *c*, *d*, *e*, *f*, *g*, and *h* indicate the proposed positions of the kinetic barriers; the evidence for these assignments is presented throughout the text. (**B**) Representative unfolding (black) and refolding (pink) force/extension curves of the L-21 RNA displaying six unfolding events (rips). The RNA is attached by RNA · DNA handles to polystyrene beads, which are manipulated by the laser tweezers. The DNA components of the handles were prepared by polymerase chain reaction from the pBR322 plasmid. The handles do not appear to affect the functional integrity of the ribozyme, as verified by standard bulk catalysis assays (*3*). Experiments were done at 298 ± 2 K in 10 mM Tris (pH = 7), 250 mM NaCl, and 10 mM $MgCl_2$ unless otherwise noted. Our first goal was to correlate the rips to the unfolding of domains and subdomains in (A). Letters and arrows correspond to the positions we assigned to the kinetic barriers as described in the text. The unfolding curve chosen here does not display barriers *d* and *g*, indicated by the dashed arrows.

[1]Department of Physics and Department of Molecular and Cell Biology and Howard Hughes Medical Institute, [2]Biophysics Graduate Group, [3]Department of Chemistry, University of California, Berkeley, CA 94720, USA. [4]Physical Biosciences Division, Lawrence Berkeley National Laboratory, Berkeley, CA 94720, USA.

*These authors contributed equally to this work.
†Present address: DuPont Company Experimental Station, Post Office Box 80328, Wilmington, DE 19880–0328, USA.
‡To whom correspondence should be addressed. E-mail: carlos@alice.berkeley.edu

the extended final state of the RNA in the pulling experiment. The superposition of the refolding curves with and without Mg^{2+} indicates that Mg^{2+} does not create barriers to formation of secondary structure. In contrast, the pronounced difference between RNA unfolding with and without Mg^{2+} reveals that the rips are likely to result from the breaking of Mg^{2+}-dependent interactions with the subsequent unzipping of secondary structure.

We used three complementary approaches to assign each rip in the force/extension curves to the unfolding of a specific RNA structure, domain, or subdomain. First, because the ribozyme domains are stable independent of their tertiary context (*16*), we could associate kinetic barriers with regions of the molecule by pulling on progressively larger pieces of L-21, ultimately reconstructing the entire molecule. Second, we assigned each rip found in the isolated L-21 domains to the unfolding of a particular subdomain by comparing the number of single-stranded nucleotides released at each rip with the known secondary structure (*3*). The number of nucleotides between two barriers was obtained from the increases in molecular extension at each rip using the wormlike chain (WLC) model (*17*). Third, we mutated specific nucleotides of the ribozyme and used antisense oligonucleotides targeted to particular interactions to confirm the assignments derived from the first two methods.

We first characterized the P4-P6 domain (Fig. 1A), whose high-resolution structure has been determined (*18*, *19*) and which includes the previously studied P5abc molecule (*1*). P4-P6 is the first higher order structure formed during assembly of the catalytically active ribozyme, and its native tertiary structure is stabilized by several specifically bound Mg^{2+} ions (*20*, *21*). P4-P6's force/extension curves are reversible in the absence of Mg^{2+}, but the unfolding curves display rips in 10 mM Mg^{2+} even at small loading rates (<3 pN s^{-1}), revealing several kinetic barriers (Fig. 2A). The most prominent barriers are labeled *f*, *g*, and *h* (*3*) (Fig. 2A; red, black, and blue WLC curves, respectively). Each barrier was assigned to a region as described above. An antisense DNA oligonucleotide was designed to hybridize with sequences involved in the tertiary contact proposed to compose barrier *f*; incubating P4-P6 with μM concentrations of this oligonucleotide eliminated rip *f* (Figs. 1A, I, and 2A, inset), thus confirming the assignment of the barrier. The barrier positions shown in Table 1 and Fig. 1A correlate with known sites of tertiary interactions (*18*) and with protection sites revealed by chemical reactivity studies (*22*). Barrier *f* is located close to the base of P6 and corresponds to a tetraloop-tetraloop receptor contact between P5b and P6 (T3). Barrier *g* at the beginning of the P5 stem corresponds to the coordination of Mg^{2+} ions close to the tertiary contact between the A-rich bulge and the P4 stem (T2). Barrier *h* at the base of the P5abc helix corresponds to the Mg^{2+}-mediated intradomain tertiary contact between the A-rich bulge and P5c (T1). The rip assigned to P5abc unfolding has force and length characteristics similar to those of P5abc unfolded alone (*1*). The three barriers were characterized as a function of Mg^{2+} concentration (fig. S5). Other more rarely observed barriers were assigned next. Four unfolding intermediates and four distinct unfolding trajectories were detected at our experimental resolution and can be represented in a mechanical unfolding map (Fig. 2B).

Incubation at low force (30 s at 2 pN) to facilitate complete refolding of the RNA before unfolding (*3*, *23*) had no effect on the force/extension curves, consistent with complete folding of P4-P6 in less than a second (*24*, *25*). Thus, the observed variation in unfolding trajectory is likely because of the stochastic nature of kinetic barrier rupture, rather than initial state heterogeneity resulting from partially folded molecules. Although not all the barriers are seen in every pull, the subdomains and domains of the molecule always unfold in the same order (Fig. 2B).

Having characterized the barriers in the P4-P6 domain, we applied similar approaches to increasingly larger pieces of RNA. The

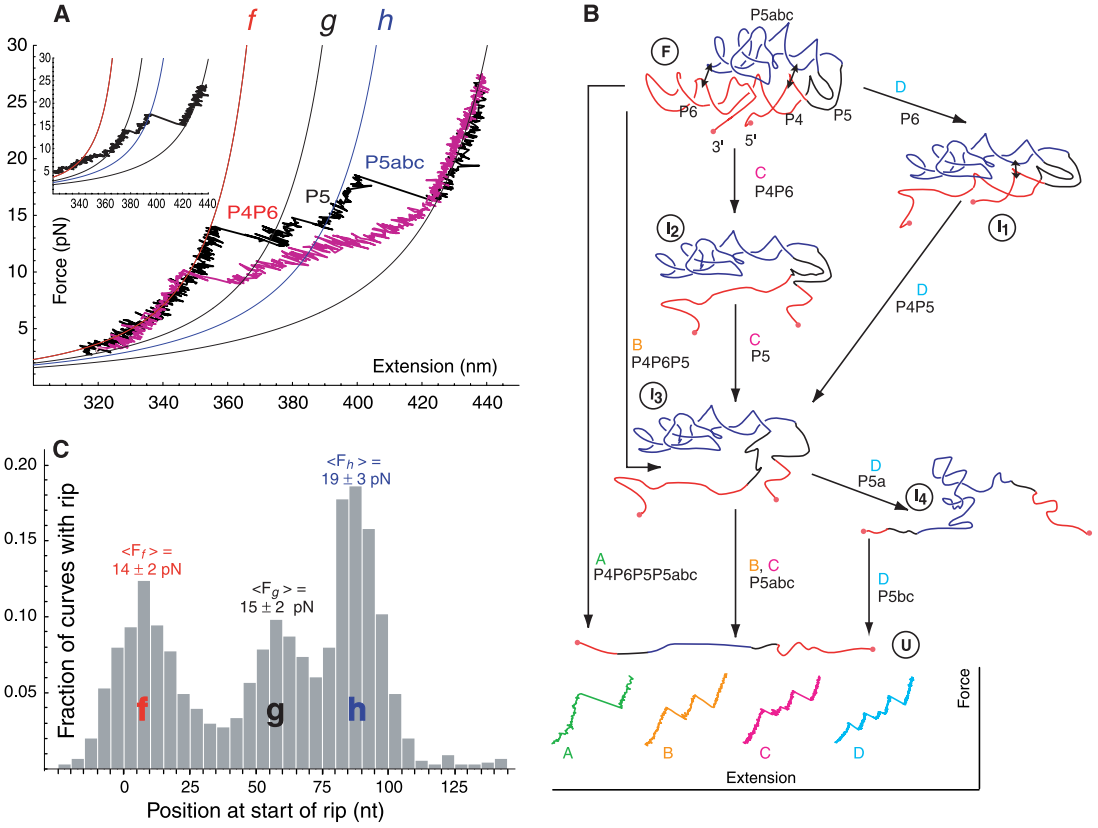

Fig. 2. (**A**) Force/extension curves for the P4-P6 domain: black, unfolding curve; pink, refolding curve. The solid lines are WLC curves for double-stranded RNA · DNA handles and an increasing number of RNA nucleotides as the unfolding progresses. The unfolding of the subdomains releases 50 nt (*f*, red, P4-P6 helices), then 30 nt (*g*, black, P5 helix), then 70 nt (*h*, blue, P5abc three-helix junction). The color code of the WLC curves corresponds to the motifs broken; it is identical to the motif color code in Fig. 1A. Inset, unfolding curves of P4-P6 in the presence of 10 μM antisense DNA oligonucleotide I (Fig. 1A), preventing T3 and disrupting barrier *f*. (**B**) Mechanical unfolding map of the P4-P6 domain. Four different unfolding trajectories were detected at our experimental resolution. F, folded; U, unfolded. I, intermediates: I_1, P6 unfolded; I_2, P6-P4 unfolded; I_3, P6-P4-P5 unfolded; I_4, P6-P4-P5-P5a unfolded. Sample force/extension curves of the different trajectories are shown in the bottom panel. Trajectory C is observed most frequently. P4-P6 colors are as in Fig. 1A. (**C**) Histogram of rips detected in 732 unfolding curves of P4-P6: position (5-nt bin), mean force (pN), and frequency of the rips.

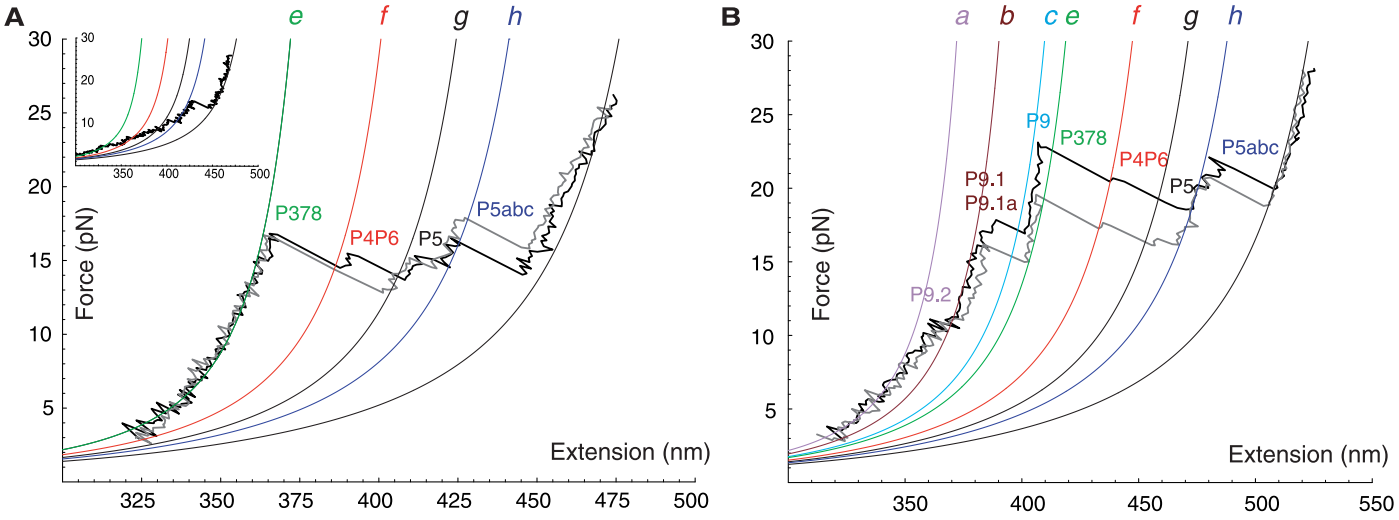

Fig. 3. (**A**) Unfolding force/extension curves of L-21ΔP9P2. Barriers *f*, *g*, and *h* are identical to those in Fig. 2A (P4-P6). The new green WLC curve (*e*) describes the barrier for unfolding of the newly added domain, P3-P8. Inset, unfolding curves of L-21ΔP2P9 in the presence of 10 μM antisense DNA oligonucleotide preventing catalytic core tertiary interactions (Fig. 1A, II). (**B**) Unfolding force/extension curve of L-21ΔP2. Characteristic barriers for the unfolding of L-21ΔP2P9 (*e* to *h*) are clearly identified. The new set of WLC curves (violet, brown, and turquoise) displays three new kinetic barriers (*a*, *b*, and *c*) present during the unfolding of the P9 extension. Barrier *a* is associated with P9.2; barrier *b*, with P9.1-P9.1a; and barrier *c*, with P9.

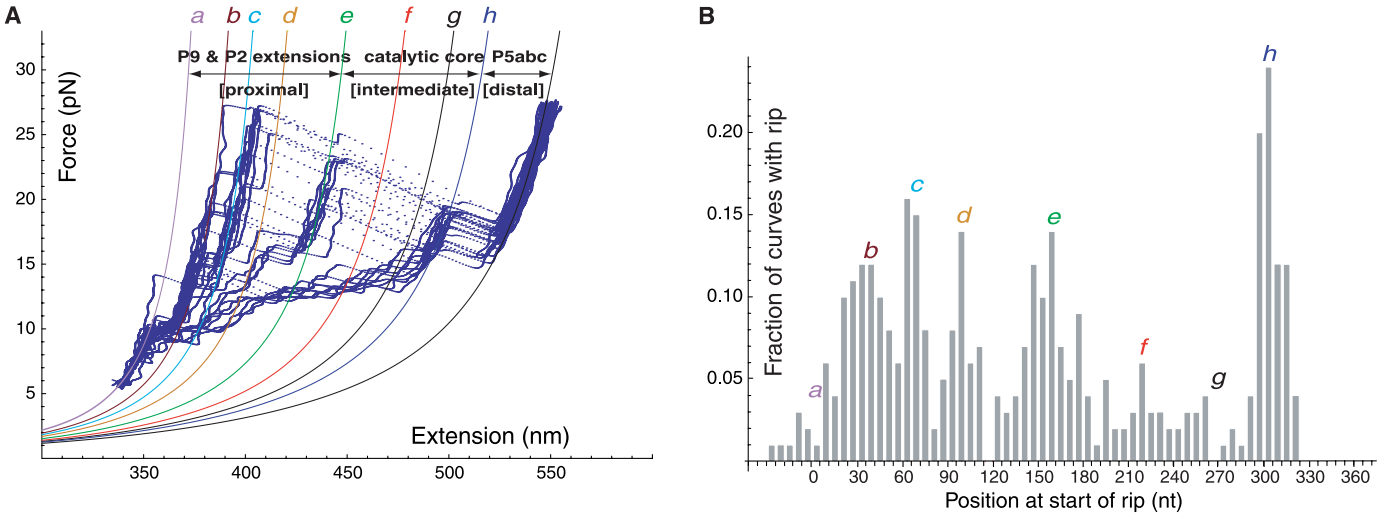

Fig. 4. (**A**) Blue curves, superposition of 32 L-21 unfolding curves displaying six of the eight kinetic barriers detected in this study. The new orange WLC curve (*d*) describes the barrier for unfolding of the newly added P2 extension. The kinetic barriers can be clustered as proximal to the beginning of unfolding (*a* to *d*, P9 and P2 extensions), intermediate (*e* to *g*, catalytic core), and distal (*h*, P5abc extension). Curves were smoothed with a Gaussian kernel. Experiments done to investigate the nature of the folded state are described in (*3*) (fig. S6). (**B**) Histogram of the rips as a function of their position for 110 curves. Letters indicate the positions of the barriers. As seen in (A), the rip corresponding to barrier *a* is very frequent but has a different slope than the other rips. Our rip detection algorithm was based on slope differences and leaves rip *a* poorly detected and poorly represented in (B).

L-21 ribozyme's catalytic core, P4-P6 plus P3-P8 (L-21ΔP2P9), shows the barriers *f*, *g*, and *h* found in P4-P6 and a new barrier, *e* (Fig. 3A, green WLC curve), assigned to the P3-P8 stem (Table 1). The addition of an antisense DNA oligonucleotide preventing catalytic core tertiary interactions (II in Fig. 1A) eliminates barriers *e* and *f* from the force/extension curves (Fig. 3A, inset), confirming these assignments. Analysis of the distribution of rupture forces of barrier *e* with increasing pulling rates shows that the catalytic core of L-21 is a "brittle" structure in which the transition state is located 1.5 ± 0.5 nm from the folded state along the reaction coordinate (*3*). This result is consistent with the cooperative interdomain interactions between the P3P7P8 and P4P5P6 stems within the catalytic core (*9*). Adding the P9 extensions (L-21ΔP2) to the previous molecule produces barriers, *a*, *b*, and *c*, corresponding to subdomains P9.2, P9.1-P9.1a, and P9, respectively (Table 1, Fig. 3B).

Finally, adding the P2 extension and the first 6 nt of P1 (internal guide sequence) yields the L-21 variant of the *T. thermophila* intron, which shows one new barrier, *d*, corresponding to the unfolding of the newly added P2 extension (Fig. 4A, Table 1). The remaining barriers have the same characteristics as they had in the smaller molecules (*26*), with one exception due to the addition of interdomain tertiary contact P13 (*27*). Localization of L-21 barriers (Table 1) was confirmed (fig. S7) except for barriers *b* to *d*, which are only confirmed to be part of the group of P2 and P9 extensions (*28*). Figure 4B is a histogram of all detected rips as a function of their position when the molecule was allowed to refold for 30 s at 2 pN before unfolding. Without the 30-s waiting period, the distribution of rips changes (*29*), suggesting that long-range tertiary interactions, such as P13 and P14 (Fig.

Table 1. Kinetic barriers that control the unfolding of the *T. thermophila* L-21 ribozyme. The total length of L-21 was taken from the first base pair at the 5′ end (nucleotide 31) to the last base pair at the 3′ end (nucleotide 406) (*31*); thus, the length of the unfolding RNA is 376 nt. The length of the domain is the number of single-stranded nucleotides expected to be released when each RNA region unfolds. The regions are color-coded in Fig. 1A.

Barrier	Length of rip (nt)	Mean rip force (pN)	Domain unfolded	Length of domain (nt)	Nature of barrier
a	38	12 ± 2	P9.2	39	Base of hairpin
*b**	25	18 ± 4	P9.1	22	G-C rich hairpin
*c**	35	21 ± 4	P9.1a & P9	14+19	P9.1a/P2.1 kissing loop (P13) P9/P5 contact (T4)
d	60	19 ± 5	P2 & P2.1	27+36	P2/P5c kissing loop (P14) P2.1/P3 contact (T5)
e	60	21 ± 3	P3-P7-P8	65	Multiple catalytic core contacts (Tcc)
f	50	16 ± 2	P4-P6	50	P5b tetraloop/P6 tetraloop receptor (T3)
g	35	15 ± 2	P4-P5	33	P5a A-rich bulge/P4 (T2)
h	73	19 ± 2	P5abc	71	P5a A-rich bulge/P5c (T1)

*Note that the lengths of rips *b* and *c* change between L-21ΔP2 (Fig. 3) and L-21 (Fig. 4A) (*32*).

1A) involving P9 and P2, form more slowly.

In the presence of Mg^{2+}, barrier *a* is unique in that it yields at low force and the molecule displays bistability. This barrier corresponds to the unfolding of the P9.2 motif, which is not involved in tertiary interactions. Under a constant force of ~11 pN, it "hops" back and forth by 15 nm between its folded and unfolded forms (Fig. 1B, barrier *a*). At a force of 11.6 pN, the apparent forward and reverse rate constants are 1.5 s^{-1} and 4.4 s^{-1}, respectively (*1*). The remaining barriers *b* to *h* yield at higher mean forces (15 to 21 pN) in Mg^{2+} (Table 1) (*30*). Thus, barriers due to secondary interactions alone, such as barrier *a*, tend to yield at low forces (below 14 pN) and unfold and refold within our time resolution of milliseconds to minutes. In contrast, barriers that involve secondary and tertiary interactions usually yield at higher forces, unfold and refold very slowly, and do not display bistability within our observation times. These barriers are rate-limiting for the unfolding of the whole ribozyme.

For the L-21 ribozyme, unfolding commences at ~12 pN, with the reversible unfolding of the P9.2 helix (Table 1). A G · C rich hairpin (P9.1) yields next, followed by breaking of several peripheral contacts (P9.1a/P2.1, P9/P5, P2/P5c, and P2.1/P3). The mechanical forces needed to break these peripheral barriers are several pN higher than the forces needed for the two hairpins (P9.1 and P9.2), probably reflecting the high transition free-energy barriers of Mg^{2+}-stabilized tertiary contacts. Once the peripheral barriers have yielded, the catalytic core is exposed to the mechanical force. The core remains folded until the force reaches ~21 pN. It then unfolds cooperatively, and ~60 nt are released. Unfolding of L-21 ends with the opening of the P4-P6 domain in a way that is indistinguishable from the unfolding of the isolated domain. The position of the handles with respect to the different domains affects the order in which the domains unfold (fig. S8).

We conclude with the following points: (i) although the overall thermodynamic stability of the molecule is determined largely by based-paired helices, the dynamics of mechanical unfolding are mainly controlled by local kinetic barriers imposed by Mg^{2+}-dependent tertiary interactions; (ii) in contrast to thermal melting, the partially unfolded intermediates encountered by molecular machines in the cell contain mixtures of secondary structures and tertiary contacts; (iii) the order of unfolding is determined by the connectivity of the molecule such that secondary structures unfold progressively as the force is applied and as their tertiary contacts are broken; and (iv) the method of assignment of kinetic barriers presented here should be of general use to analyze the mechanical unfolding of other complex RNA structures.

References and Notes

1. J. Liphardt, B. Onoa, S. B. Smith, I. Tinoco Jr., C. Bustamante, *Science* **292**, 733 (2001).
2. S. B. Smith, Y. Cui, C. Bustamante, *Methods Enzymol.* **361**, 134 (2003).
3. Materials and methods are available as supporting material on *Science* Online.
4. X. Zhuang *et al*., *Science* **288**, 2048 (2000).
5. R. Russell *et al*., *Proc. Natl. Acad. Sci. U.S.A.* **99**, 155 (2002).
6. The L-21 derivative of this molecule lacks its native substrates (exons) but catalyzes the cleavage of substrate RNAs provided in trans.
7. A. J. Zaug, C. A. Grosshans, T. R. Cech, *Biochemistry* **27**, 8924 (1988).
8. D. K. Treiber, J. R. Williamson, *Curr. Opin. Struct. Biol.* **11**, 309 (2001).
9. B. L. Golden, A. R. Gooding, E. R. Podell, T. R. Cech, *Science* **282**, 259 (1998).
10. V. Lehnert, L. Jaeger, F. Michel, E. Westhof, *Chem. Biol.* **3**, 993 (1996).
11. D. Thirumalai, N. Lee, S. A. Woodson, D. K. Klimov, *Ann. Rev. Phys. Chem.* **52**, 751 (2001).
12. U. Bockelmann, B. Essavez-Roulet, F. Heslot, *Phys. Rev. E* **58**, 286 (1998).
13. U. Bockelmann, P. Thomen, B. Essevaz-Roulet, V. Viasnoff, F. Heslot, *Biophys. J.* **82**, 1537 (2002).
14. U. Gerland, R. Bundschuh, T. Hwa, *Biophys. J.* **81**, 1324 (2001).
15. _____, *Biophys. J.*, in press; preprint available at http://arxiv.org/abs/cond-mat/0208202.
16. I. Tinoco Jr., C. Bustamante, *J. Mol. Biol.* **293**, 271 (1999).
17. C. Bustamante, J. F. Marko, E. D. Siggia, S. B. Smith, *Science* **265**, 1599 (1994).
18. J. H. Cate *et al*., *Science* **273**, 1678 (1996).
19. K. Juneau, E. Podell, D. J. Harrington, T. R. Cech, *Structure* **9**, 221 (2001).
20. B. Sclavi, M. Sullivan, M. R. Chance, M. Brenowitz, S. A. Woodson, *Science* **279**, 1940 (1998).
21. P. P. Zarrinkar, J. R. Williamson, *Science* **265**, 918 (1994).
22. C. Y. Ralston, Q. He, M. Brenowitz, M. R. Chance, *Nature Struct. Biol.* **7**, 371 (2000).
23. The reasons for choosing a waiting time of 30 s at 2 pN are as follows: In vitro and under similar ionic and temperature conditions, P4-P6 folds at a rate of 4.7 s^{-1}. Here, we let P4-P6 refold for 30 s (two orders of magnitude longer than stated above) to favor complete refolding of the molecule. We compared P4-P6 refolding at 0, 2, 4, and 6 pN and observed no substantial differences in unfolding curves. We chose 2 pN because it allowed complete refolding but minimized nonspecific interactions and the attachment of additional molecules between the two beads.
24. Mechanical unfolding of P4-P6 after 0 s (732 curves) and 30 s (323 curves) of refolding both displayed three barriers. The barriers were within 5 nt of each other, the frequencies of arrest at the barriers were within 7% of each other, and the rupture forces were within 2 pN of each other.
25. S. K. Silverman, M. L. Deras, S. A. Woodson, S. A. Scaringe, T. R. Cech, *Biochemistry* **39**, 12465 (2000).
26. Independent of the context of the barriers, their rupture forces and position are constant to within 2 pN and 5 nt, respectively. For example, P5abc ruptures at 19 pN in the context of both P4-P6 (Fig. 2C) and L-21 (Fig. 4B) and releases 70 nt in P4-P6 and 73 in L-21.
27. The lengths of rips *b* and *c* change between L-21ΔP2 (Fig. 3) and L-21 (Fig. 4A). Rip *b* is longer than *c* in L-21ΔP2, and rip *c* is longer than *b* in L-21. When P2 is added to L-21ΔP2 to yield L-21, the P13 interaction now takes place between P9.1a and P2.1, causing P9.1a to rupture at the same time as P9 instead of at the same time as P9.1.
28. Similar lengths for motifs P9, P9.1, P9.1a, P.2, and P2.1, and their interactions (P13, P14, and T4; Fig. 1A), make precise localization of barriers *b*, *c*, and *d* difficult. However, from our analysis we propose that barrier *b* corresponds to P9.1; barrier *c*, to P9-P9.1a; and barrier *d*, to P2-P2.1. Site-directed mutagenesis and/or varying the lengths of these motifs could help verify the proposed barrier localizations.
29. Without the 30-s refolding period, the frequencies of arrest at barriers *b*, *c*, and *d* are all below 0.05 and thus lower than the frequency of arrest at barrier *e* (catalytic core). In contrast, with the 30-s refolding period (Fig. 4B), frequencies of arrest at those barriers are comparable to frequency of arrest at barrier *e*.
30. Barriers *b* to *h* involve secondary and tertiary contacts, with the exception of P9.1, which does not make tertiary contacts but has a high GC content. Data not shown here revealed that a high GC content is associated with high rupture forces and a lack of detectable bistability in current experimental conditions (*31*).
31. J. Liphardt, unpublished observations.
32. R. T. Batey, R. P. Rambo, J. A. Doudna, *Angew. Chem. Int. Ed.* **38**, 2326 (1999).

33. This research was supported in part by NIH grants GM-10840 and GM-32543, Department of Energy grants DE-FG03-86ER60406 and DE-AC03-76DF00098, and NSF grants MBC-9118482 and DBI-9732140. B.O. and J.L. were supported by the Program in Mathematics and Molecular Biology through a Burroughs Wellcome Fund Fellowship, and S.D. is supported by the Natural Sciences and Engineering Research Council of Canada and Fonds pour la Formation de Chercheurs et l'Aide à la Recherche du Québec. We thank J. McCoy for work with L-21 mutants; P. Gorostiza for helpful suggestions; and S. Woodson for encouragement, helpful discussions, and multiple constructs.

Supporting Online Material

www.sciencemag.org/cgi/content/full/299/5614/1892/DC1
Materials and Methods
Figs. S5 to S8
References and Notes

9 December 2002; accepted 24 February 2003